12th IFAC International Symposium on
Advanced Control of Chemical Processes
July 14-17, 2024. Toronto, Canada

Robust and Simple Output Predictive Control for HEV Energy Management ⋆

R. Nozaki * **K. Sakamoto** * **I. Mizumoto** **

* *Graduate School of Science and Technology, Kumamoto University, Kumamoto, Japan.*
** *Faculty of Advanced Science and Technology, Kumamoto University, Kumamoto, Japan (e-mail: ikuro@gpo.kumamoto-u.ac.jp)*

Abstract: Power-split HEVs can improve their overall fuel economy by applying an appropriate energy management strategy. One of the most popular energy management strategies is model predictive control (MPC) which has attracted a great deal of attention in the HEV research community. In this paper, we focus on the energy management of HEVs and propose a novel energy management system using a new robust predictive control based on almost strictly positive real properties. We also verify that the proposed method can improve fuel efficiency compared with the existing rule-based control through numerical simulations.

Keywords: Energy Management, Hybrid Electric Vehicle, Robust Predictive Control, Power-Split HEV, Fuel Economy

1. INTRODUCTION

In recent years, hybrid electric vehicles (HEVs) have attracted a great deal of attention as a means to realize a sustainable low-carbon society (Sciarretta and Guzzella, 2007a). The optimization method for this energy allocation is called Energy Management Strategy (EMS), and various methods have been proposed (Tran et al., 2020).

In particular, methods based on model predictive control (MPC) have attracted much attention in the HEV research community (Huang et al., 2017). MPC determines the optimal input so as to minimize a given cost function sequentially, using a HEV numerical model to predict future states (Camacho and Bordons, 2007; Clarke et al., 1987). However, generally, MPC has the following characteristics and problems.

- Control performance deteriorates in the presence of uncertainties such as modeling errors and disturbances.
- The controller design process becomes more complex for systems with the higher order because the MPC requires states of the controlled system.
- In many cases, the optimal input is obtained numerically using an iterative method, which is computationally demanding for on-board calculation.

To solve the above problem, a robust and simple output predictive control (OPC) method with a parallel feedforward compensator (PFC) has been proposed (Fujii and Mizumoto, 2017; Mizumoto et al., 2018). This method realizes a robust and computationally inexpensive OPC by introducing a PFC to ensure the Almost Strictly Positive Real (ASPR) properties of the system. Using this ASPR-augmented system with a PFC, one can construct a predictive control system with a simple first-order predictor. In particular, continuous-time robust output predictive control proposed in Mizumoto et al. (2018) has been applied to energy management strategies for HEVs and shown to be effective (Nozaki et al., 2024). However, the results in Nozaki et al. (2024) were obtained in the case where the control system was configured assuming that the unknown future driver demand power is constant, but in practical case, the driver's requirements change significantly depending on driving conditions. Therefore, control of the energy management system may perform better by predicting future driver demand power in real time.

In this regard, Sun et al. (2015); Hara et al. (2016); Xiang et al. (2017) have proposed various forms of future driver demand prediction methods including velocity and power, and have achieved improvement in fuel economy by designing MPCs with predicted driver demands. However, as mentioned before, the general MPC algorithms used in these proposals may have problems in terms of computational load and tolerance to uncertainty.

In this paper, we propose an energy management strategy for HEVs based on robust and simple OPC using a real-time driver demand predictor. In numerical simulations, we use a power-split HEV model (No. 20008) provided by the Japan Automotive Model-Based Engineering Center (JAMBE). This model is a guideline-compliant model created by the Ministry of Economy, Trade and Industry "Simulation infrastructure construction project for accelerating development of next-generation vehicles (2018-2020)" and JAMBE (from 2021). Various studies have been conducted using this model as a benchmark.

⋆ This paper is obtained as a result of a grant project (JPNP21014) conducted by The Research association of Automotive Internal Combustion Engines (AICE) with support from the New Energy and Industrial Technology Development Organization (NEDO).

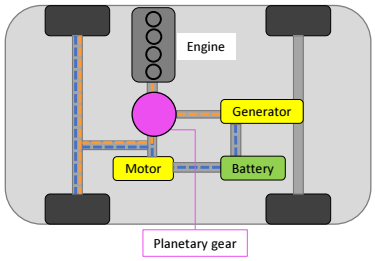

Fig. 1. Power-Split HEV

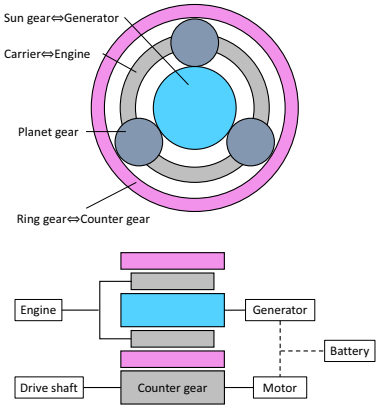

Fig. 2. Planetary Gear

2. HEV MODEL

This paper deals with a power-split HEV as shown in Fig. 1. The power-split HEV has an engine and two motors, and their power is divided by planetary gear. In the following, we consider modeling the power-split HEV but derive only the models used to design the control system. For the detailed model derivation, refer to Nozaki et al. (2024); Borhan et al. (2012); Sciarretta and Guzzella (2007b).

2.1 Planetary Gear

In a power-split HEV, a planetary gear plays an important role in splitting the power between the engine, motor, and generator, as shown in Fig.2. The planetary gear characteristics allow the rotational speed equation to be expressed as follows.

$$R_s w_s(t) + R_r w_r(t) = (R_s + R_r) w_c(t) \quad (1)$$
$$w_s(t) = w_{gen}(t) \quad (2)$$
$$w_c(t) = w_{eng}(t) \quad (3)$$
$$w_r(t) = \alpha w_{co}(t) \quad (4)$$
$$w_{mot}(t) = \beta w_{co}(t) \quad (5)$$

where R_s[m], R_r[m] are the radius of the sun gear and the inner radius of the ring gear, respectively, $w_s(t)$[rad/s], $w_r(t)$[rad/s], $w_c(t)$[rad/s] and $w_{co}(t)$[rad/s] are the rotational speeds of the sun gear, ring gear, carrier, and counter gear. Also, $w_{gen}(t)$[rad/s], $w_{eng}(t)$[rad/s], and $w_{mot}(t)$[rad/s] are the rotation speed of the generator, engine, and motor. α is the radius ratio of the counter gear to the outer radius of the ring gear, and β is the radius ratio of the counter gear to the radius of the motor gear.

The following relation holds for the vehicle speed and the rotational speed of the counter gear.

$$w_{co}(t) = \frac{G_f}{R_w} V(t) \quad (6)$$

G_f is the differential gear ratio, R_w[m] is the tire radius, and $V(t)$[m/s] is the vehicle speed. Furthermore, from (1)∼(6), $w_{mot}(t)$ and $w_{gen}(t)$ can be transformed as follows.

$$w_{gen}(t) = \frac{R_s + R_r}{R_s} w_{eng}(t) - \frac{R_r \alpha G_f}{R_s R_w} V(t) \quad (7)$$
$$w_{mot}(t) = \frac{\beta G_f}{R_w} V(t) \quad (8)$$

Next, we derive the equations of angular motion for the generator, engine, and motor. Neglecting the inertial force of the planet gear and assuming that all the connecting axes of the powertrain are rigid, the equations of angular motion can be obtained as follows (Borhan et al., 2012).

$$\begin{aligned} I_{gen}\dot{w}_{gen}(t) &= T_{gen}(t) + F(t) \times R_s \\ I_{eng}\dot{w}_{eng}(t) &= T_{eng}(t) - F(t) \times (R_s + R_r) \\ I_{mot}\frac{\dot{w}_{mot}(t)}{\beta} &= \alpha(F(t) \times R_r) + \beta T_{mot}(t) - \frac{T_{driver}(t)}{G_f}, \end{aligned} \quad (9)$$

where I_{gen}[kgm^2], I_{eng}[kgm^2], I_{mot}[kgm^2] are the inertia of the generator, engine and motor. $T_{gen}(t)$[Nm], $T_{eng}(t)$[Nm], $T_{mot}(t)$[Nm] are the torque of generator, engine and motor. $T_{driver}(t)$[Nm] is the driver's torque demand and $F(t)$[N] is the interaction force with the planetary gear.

Here, since the rotational dynamics are much faster than the battery dynamics and the effect of inertia on the battery dynamics is limited, the inertia losses of generator, engine and motor $I_{gen}\dot{w}_{gen}(t), I_{eng}\dot{w}_{eng}(t)$, and $I_{mot}\frac{\dot{w}_{mot}(t)}{\beta}$ can be ignored. Thus, the following two equations hold from (9) (Borhan et al., 2012) by ignoring the inertia losses of the generator, engine and motor.

$$T_{gen}(t) = -\frac{R_s}{R_s + R_r} T_{eng}(t) \quad (10)$$
$$T_{mot}(t) = -\frac{\alpha}{\beta}\frac{R_r}{R_s + R_r} T_{eng}(t) + \frac{1}{\beta G_f} T_{driver}(t) \quad (11)$$

2.2 Battery

The battery State of Charge (SOC) is an important state variable in the control of HEVs and its dynamics is expressed by the following equation (Sciarretta and Guzzella, 2007b).

$$\dot{soc}(t) = -\frac{U_{oc}(soc) - \sqrt{U_{oc}^2(soc) - 4R(soc)P_{bat}(t)}}{2Q_{max}R(soc)} \times 100 \quad (12)$$

where $soc(t)$[%] is the battery state of charge, Q_{max}[Ah] is the battery capacity, $P_{bat}(t)$[W] is the battery power, $U_{oc}(soc)$[V] is the open circuit voltage and $R(soc)$[Ω] is the internal resistance. $U_{oc}(soc)$ and $R(soc)$ depend on $soc(t)$. Furthermore, the following equation holds between the battery power $P_{bat}(t)$, the engine power $P_{eng}(t)$, and the driver power demand $P_{driver}(t)$ from (7) (8) (10) (11)

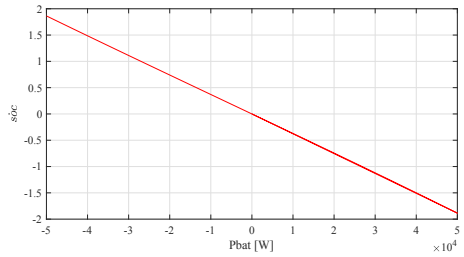

Fig. 3. $\dot{soc}$ and P_{bat}

(Nozaki et al., 2024). However, for simplicity, the power loss during charging and discharging is not considered in this relation.

$$\begin{aligned} P_{bat}(t) &= T_{gen}(t)w_{gen}(t) + T_{mot}(t)w_{mot}(t) \\ &= \left(-\frac{R_s}{R_s+R_r}T_{eng}(t)\right)\left(\frac{R_s+R_r}{R_s}w_{eng}(t) - \frac{R_r\alpha G_f}{R_s R_w}V(t)\right) \\ &\quad + \left(-\frac{\alpha}{\beta}\frac{R_r}{R_s+R_r}T_{eng}(t) + \frac{1}{\beta G_f}T_{driver}\right)\left(\frac{\beta G_f}{R_w}V(t)\right) \\ &= -T_{eng}(t)w_{eng}(t) + \frac{V(t)}{R_w}T_{driver}(t) \\ &= -P_{eng}(t) + P_{driver}(t) \end{aligned} \tag{13}$$

In the HEV model treated in this paper, the relation between $\dot{soc}(t)$ and $P_{bat}(t)$ calculated from (12) is generally linear in the region where the SOC operating point is $50 \leqq soc(t) \leqq 70$ and $-5 \times 10^4 \leqq P_{bat}(t) \leqq 5 \times 10^4$ (the region used in numerical simulations in Chapter 5), as shown in Fig. 3. Therefore, if the slope is given by $-S_o(< 0)$, the relation between the rate of change of SOC and battery power can be expressed as follows:

$$\dot{soc}(t) = -S_o P_{bat}(t) \tag{14}$$

Furthermore, considering the relation given in (13), the following model between the rate of change of SOC and engine power can be obtained.

$$\dot{soc}(t) = S_o(P_{eng}(t) - P_{driver}(t)) \tag{15}$$

2.3 Engine

We consider only the part related to fuel consumption, and detailed dynamics are not considered. In the HEV model used in this paper, instantaneous fuel consumption $\dot{m}_f(t)$[g/s] is expressed as a function of engine torque $T_{eng}(t)$ and engine speed $w_{eng}(t)$, and is represented by MAP. Using this MAP data, one can obtain the relation between instantaneous fuel consumption $\dot{m}_f(t)$ and engine power $P_{eng}(t)$ as shown in Fig. 4, and a linear relation can be found between these two parameters. If the slope of the relation is given by η, the following relation is obtained.

$$\dot{m}_f(t) = \eta P_{eng}(t) \tag{16}$$

Note that the value of η is assumed to be unknown in the controller design. We only assume that the relation between instantaneous fuel consumption $\dot{m}_f(t)$ and engine power $P_{eng}(t)$ is linear.

3. PROBLEM SETUP

3.1 Objective

The objective of energy management in this paper is to minimize fuel consumption while maintaining SOC. The

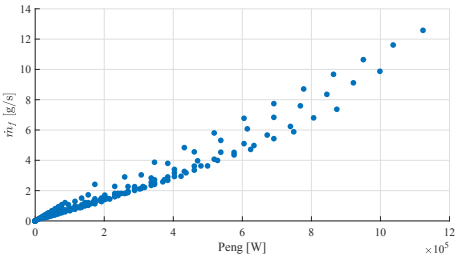

Fig. 4. Fuel consumption

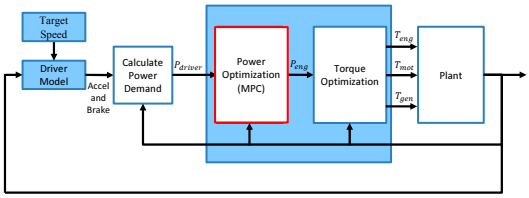

Fig. 5. Overview of the controller

problem is also simplified by making the controller hierarchical, as shown in Fig. 5 in this paper. The Power Optimization controller calculates the optimal value of engine power $P_{eng}(t)$ based on the driver power demand $P_{driver}(t)$ calculated upstream. Then, the torque of the engine, motor, and generator is calculated by the Torque Optimization controller based on the obtained optimal value of engine power $P_{eng}(t)$. In this paper, we propose a robust and simple OPC that is used as a Power Optimization Controller, and a sample controller (rule-based control) given in the JAMBE HEV model (No. 20008) is used in the Torque Optimization controller.

3.2 Assumptions on Controlled System

Here, we consider the engine power $P_{eng}(t)$ as input, the driver power demands $P_{driver}(t)$ as disturbance, and the battery state of charge $soc(t)$ as output, and consider designing a control system using the battery dynamics equation (15). The control system is designed provided that the following assumptions are satisfied for the SOC system (15).

Assumption 1. For the system (15), there exists a stable parallel feedforward compensator (PFC) $H_{est}(s)$ shown in Fig.6, which has a state space representation of

$$\begin{aligned} \dot{\boldsymbol{x}}_{fp}(t) &= A_{fp}\boldsymbol{x}_{fp}(t) + \boldsymbol{b}_{fp}\bar{u}(t) \\ y_{fp}(t) &= \boldsymbol{c}_{fp}^T\boldsymbol{x}_{fp}(t)\ , \end{aligned} \tag{17}$$

such that the resulting augmented system shown in Fig.6:

$$\begin{aligned} \dot{\boldsymbol{x}}_{ap}(t) &= A_{ap}\boldsymbol{x}_{ap}(t) + \boldsymbol{b}_{ap}\bar{u}(t) \\ y_{ap}(t) &= \boldsymbol{c}_{ap}^T\boldsymbol{x}_{ap}(t) \end{aligned} \tag{18}$$

with

$$\boldsymbol{x}_{ap}(t) = \begin{bmatrix} soc(t) \\ \boldsymbol{x}_{fp}(t) \end{bmatrix}\ ,\ A_{ap} = \begin{bmatrix} 0 & \boldsymbol{0}^T \\ \boldsymbol{0} & A_{fp} \end{bmatrix}$$

$$\boldsymbol{b}_{ap} = \begin{bmatrix} S_o \\ \boldsymbol{b}_{fp} \end{bmatrix}\ ,\ \boldsymbol{c}_{ap} = \begin{bmatrix} 1 \\ \boldsymbol{c}_{fp} \end{bmatrix}$$

$$\bar{u}(t) = P_{eng}(t) - P_{driver}(t)$$

is ASPR, i.e. it has a relative degree of 1 and is minimum-phase.

Assumption 2. The disturbance $P_{driver}(t)$ (the current driver demand power) is measurable and available.

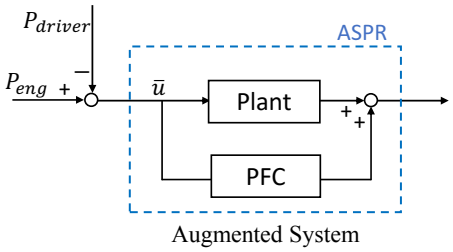

Fig. 6. Augmented system

Remark: Although the modeled battery system itself is ASPR, we are considering introducing a PFC that satisfies Assumption 1 for the purpose of ensuring the ASPR-ness of the practical system including uncertainty.

4. CONTROLLER DESIGN

4.1 Augmented Output Estimator

We first consider designing an output estimator for the given ASPR augmented system (18) under Assumption 1.

Since the augmented system (18) has a relative degree of 1 and minimum-phase, there exists a nonsingular transformation $\left[y_{ap}(t) \;\; \boldsymbol{\eta}^T(t)\right]^T = \Phi \boldsymbol{x}_{ap}(t)$ such that (18) is transformed into the following canonical form (Isidori, 1995):

$$\begin{aligned} \dot{y}_{ap}(t) &= a_a^* y_{ap}(t) + b_a^* \bar{u}(t) + \boldsymbol{c}_\eta^T \boldsymbol{\eta}(t) \\ \dot{\boldsymbol{\eta}}(t) &= A_\eta \boldsymbol{\eta}(t) + \boldsymbol{b}_\eta y_{ap}(t) \end{aligned} \tag{19}$$

where a_a^* and b_a^* are unknown parameters but their nominal values a_a and b_a are assumed to be known, and the zero dynamics: $\dot{\boldsymbol{\eta}}(t) = A_\eta \boldsymbol{\eta}(t)$ is stable from the minimum-phase property of the augmented system.

Rewrite the system(19) using the nominal value a_a and b_a of a_a^* and b_a^* as

$$\dot{y}_{ap}(t) = a_a y_{ap}(t) + b_a \bar{u}(t) + f(t) \tag{20}$$

$$f(t) = \Delta a_a y_{ap}(t) + \Delta b_a \bar{u}(t) + \boldsymbol{c}_\eta^T \boldsymbol{\eta}(t) \tag{21}$$

with $\Delta a_a = a_a^* - a_a,\ \Delta b_a = b_a^* - b_a$.

Based on this representation of the augmented system (20), we design an output estimator for the augmented system as follows(Mizumoto et al., 2018):

$$\begin{aligned} \dot{z}_1(t) &= a_a z_1(t) + b_a \bar{u}(t) + z_2(t) \\ &\quad + k_1(y_{ap}(t) - z_1(t)) \end{aligned} \tag{22}$$

$$\dot{z}_2(t) = k_2(y_{ap}(t) - z_1(t)) \ , \tag{23}$$

where $z_1(t)$ is the estimated value of $y_{ap}(t)$ and $z_2(t)$ is the estimated value of $f(t)$. k_1 and k_2 are design parameters and they are set such that

$$A_o = \begin{bmatrix} a_a - k_1 & 1 \\ -k_2 & 0 \end{bmatrix} \tag{24}$$

is a stable matrix.

4.2 Output Predictor Design

An output predictor for the augmented output is designed according to the designed output estimator (22) as follows:

$$\begin{aligned} \frac{\partial \hat{\bar{y}}_{ap}(t,\tau)}{\partial \tau} &= a_a \hat{\bar{y}}_{ap}(t,\tau) + b_a \bar{u}(t,\tau) + z_2(t,0) \\ &= a_a \hat{\bar{y}}_{ap}(t,\tau) + b_a P_{eng}(t,\tau) \\ &\quad - b_a P_{driver}(t,\tau) + z_2(t,0) \end{aligned} \tag{25}$$

$$\hat{\bar{y}}_{ap}(t,0) = z_1(t,0)$$

where $\tau (0 \le \tau \le t_f)$ in (t,τ) denotes the predicted time from the current time t, and t_f is a terminal time. $P_{eng}(t,\tau)$ is a predictive input to be determined later in the following section 4.3, and $P_{driver}(t,\tau)$ is a future driver power demand predicted by a power demand predictor given in section 4.4.

The output predictor designed above is the one for the augmented system given in (18). Based on this output predictor, the practical predicted output can be obtained by

$$\begin{aligned} \hat{soc}(t,\tau) &= \hat{\bar{y}}_{ap}(t,\tau) - y_{fp}(t,\tau) \\ &= \hat{\bar{y}}_{ap}(t,\tau) - \boldsymbol{c}_{fp}^T \boldsymbol{x}_{fp}(t,\tau) \\ &= \bar{\boldsymbol{c}}_{ap}^T \bar{\boldsymbol{x}}_{ap}(t,\tau) \end{aligned} \tag{26}$$

$$\bar{\boldsymbol{c}}_{ap}^T = \left[\, 1 \ , \ -\boldsymbol{c}_{fp}^T \,\right] \ , \ \bar{\boldsymbol{x}}_{ap}(t,\tau) = \begin{bmatrix} \hat{\bar{y}}_{ap}(t,\tau) \\ \boldsymbol{x}_{fp}(t,\tau) \end{bmatrix}$$

Moreover, concerning $\bar{\boldsymbol{x}}_{ap}(t,\tau)$, $\bar{\boldsymbol{x}}_{ap}$-system can be represented from (17) and (25) by

$$\frac{\partial \bar{\boldsymbol{x}}_{ap}(t,\tau)}{\partial \tau} = \bar{A}_{ap} \bar{\boldsymbol{x}}_{ap}(t,\tau) + \bar{B}_{ap} \bar{\boldsymbol{u}}_{ap}(t,\tau) \tag{27}$$

$$\bar{A}_{ap} = \begin{bmatrix} a_a & \boldsymbol{0}^T \\ \boldsymbol{0} & A_{fp} \end{bmatrix} \ , \ \bar{B}_{ap} = \begin{bmatrix} b_a & -b_a & 1 \\ \boldsymbol{b}_{fp} & -\boldsymbol{b}_{fp} & \boldsymbol{0} \end{bmatrix}$$

$$\bar{\boldsymbol{u}}_{ap}(t,\tau) = \begin{bmatrix} P_{eng}(t,\tau) \\ P_{driver}(t,\tau) \\ z_2(t,0) \end{bmatrix}$$

4.3 Cost Function Design

This section outlines the design guidelines for the predictive input $P_{eng}(t,\tau)$. The cost function that satisfies the energy management objective (minimizing fuel consumption while maintaining SOC) is given by (Nozaki et al., 2024)

$$\begin{aligned} J(t) = &\frac{1}{2} \bar{\boldsymbol{x}}_{ap}^T(t,t_f) P_f \bar{\boldsymbol{x}}_{ap}(t,t_f) \\ &+ \int_0^{t_f} \frac{1}{2} \left\{ q \hat{\bar{e}}(t,\tau)^2 + r P_{eng}(t,\tau)^2 \right\} d\tau \end{aligned} \tag{28}$$

$$\hat{\bar{e}}(t,\tau) = \hat{soc}(t,\tau) - soc_m(t+\tau)$$

under the terminal constraint:

$$\hat{\bar{e}}(t,t_f) = \hat{soc}(t,t_f) - soc_m(t+t_f) = 0 \tag{29}$$

where soc_m is the target value to track the SOC, P_f is a positive definite symmetric weight matrix, q, r are weights, and t_f is the prediction time. For the specific derivation of $P_{eng}(t,\tau)$, refer to the result obtained in Mizumoto et al. (2018). The control input to the actual control target is given as follows

$$P_{eng}(t) = P_{eng}(t,0) \tag{30}$$

4.4 Power Demand Predictor

As the situation changes from moment to moment, it is difficult to accurately predict future power demand. Therefore, to obtain an intuitive understanding of the relation

between predicted future demand power and total fuel consumption, exponentially varying velocity demand predictor has been considered in (Sun et al., 2015). However, since this method was just for intuitively understanding the relationship between future driver demand prediction and fuel consumption, there was no basis for prediction. Therefore, we propose a new prediction strategy based on a last moving average of the gradient of driver demand power that utilizes the average gradient of past driver demand powers. Thus, in each receding horizon, the gradient of driver demand power is predicted as follows:

$$\dot{P}_{driver}(t,\tau) = a(t) \times \varepsilon^{b\tau} \tag{31}$$

where $a(t)$ is the moving average of the gradient (in this research, we set the moving average over 2 seconds), $0 < \varepsilon < 1$ is the exponential coefficient, and $b > 1$ is a weighted index coefficient. Different ε are considered to examine the sensitivity of fuel economy to the predicted future power demand. We call this predictor "gradient-exponential-varying demand predictor". Since the future gradient would be unknown, we assumed that the future gradient gradually decreases.

5. NUMERICAL VALIDATION

The proposed output predictive control method with predicted driver power demand is validated through numerical simulations. We use a power-split HEV model (No. 20008) provided by the Japan Automotive Model-Based Engineering Center (JAMBE). As described in the previous section (see Fig. 5), the controllers in the power-split HEV are hierarchical, with the power optimization controller and the torque optimization controller. We design the power optimization controller by applying the proposed method and the torque optimization controller is constructed using a sample controller given in the HEV model (No. 20008).

The power optimization controller with the proposed output predictive control is designed under the following conditions:

We first assume that the nominal SOC model $G_{nom}(s)$ which is required for designing PFC is given as follows.

$$G_{nom}(s) = \frac{3.6682 \times 10^{-5}}{s} \tag{32}$$

based on the data shown in Fig. 3.

Furthermore, an augmented system $G_{est}(s)$ that satisfies Assumption 1 is given as follows.

$$G_{est}(s) = \frac{s + 3.6682 \times 10^{-8}}{s^2 + 10^{-3}s} \tag{33}$$

From the augmented system given above, the PFC $H_{est}(s)$ is obtained using the model-based design method as follows.

$$H_{est}(s) = G_{est}(s) - G_{nom}(s) \tag{34}$$

The design parameters of the control system are set as

$$k_1 = 1 \times 10^1 \ , k_2 = 1 \times 10^1$$
$$P_f = I \ , q = 1 \times 10^{-10} \ , r = 1 \times 10^7$$
$$\text{sampling time} = 2.5 \times 10^{-3}[\text{s}] \ , t_f = 20[\text{s}]$$

Moreover, a_a, b_a are obtained as follows by seeking the canonical form realization of $G_{est}(s)$ given in (33) (Isidori, 1995).

$$a_a = -9.9996 \times 10^{-4} \ , b_a = 1$$

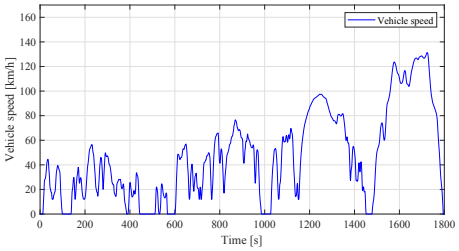

Fig. 7. Target vehicle speed (WLTC Class3b)

Table 1. Fuel consumption and Percent change

WLTC Class3b		
Rule Base	30.04 [km/L]	
Exponential Coefficient	Robust MPC	
$\varepsilon = 0$	32.34 [km/L]	7.66 [%]
$\varepsilon = 0.1$	32.45 [km/L]	8.02 [%]
$\varepsilon = 0.3$	32.72 [km/L]	8.92 [%]
$\varepsilon = 0.5$	32.82 [km/L]	9.25 [%]
$\varepsilon = 0.7$	32.99 [km/L]	9.82 [%]
$\varepsilon = 0.8$	32.56 [km/L]	8.39 [%]

In the driver demand power predictor given in (31), we set $b = 4$ for the given exponential coefficients ε.

Numerical simulations were performed with the above settings.

Note that fuel consumption is calculated under the Charge Sustainable condition (where the initial and final SOC values are matched so that energy can be discussed only in terms of fuel consumption without considering SOC).

The driving cycle used in this study (WLTC Class3b) is shown in Fig. 7.

It is worth noting that the optimal solution of (28) with terminal condition (29) can be solved analytically (Mizumoto 2018). That is, we don't have to worry about calculation time for on-board calculation.

Table 1 shows that the fuel consumption and the rate of change in fuel consumption while running for the given driving cycle as in Fig. 7 with different exponential coefficients ε. Here, the rate of change is based on the fuel consumption with the conventional rule base method. Note that we have better energy management results compared with the rule-based method as shown in Table 1 by using the proposed output predictive control method even though we set $\varepsilon = 0$.

The results shown in Table 1 say that using $P_{driver}(t,\tau)$ predicted by the gradient-exponential-varying demand predictor, the fuel consumption always improves compared with the case where the driver demand power is set at a constant ($\varepsilon = 0$) in the prediction horizon. The best result is obtained when $\varepsilon = 0.7$.

Fig.8 shows the simulation results of the WLTC Class3b using the proposed method with $\varepsilon = 0.7$ and Fig.9 shows the simulation results of the WLTC Class3b using rule-based control. From Fig.8, we can see that the SOC is maintained at the target value of SOC.

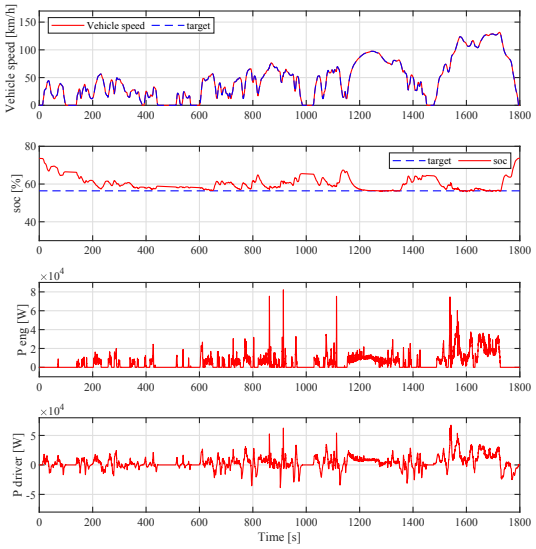

Fig. 8. Results of Robust MPC [$\varepsilon = 0.7$]

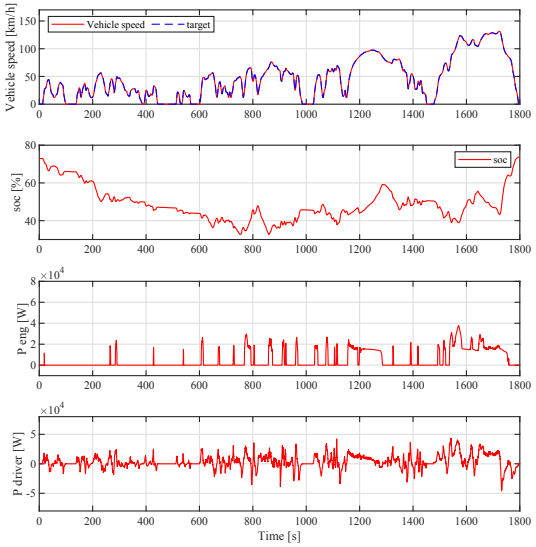

Fig. 9. Results of Rule Base method

6. CONCLUSION

We proposed an energy management strategy for HEVs based on robust and simple OPC using a novel real-time driver power demand predictor. The proposed method can handle energy management of a power-split HEV with an objective in which the SOC is kept at the desired value and the engine power is kept small. The effectiveness of the proposed method was confirmed through numerical simulations by a power-split HEV model (No. 20008) provided by the Japan Automotive Model-Based Engineering Center (JAMBE), and very good results were obtained compared with the conventional MAP control and original output predictive control without driver power demand predictor.

REFERENCES

Borhan, H., Vahidi, A., Phillips, A., Kuang, M., Kolmanovsky, I., and Cairano, S. (2012). Mpc-based energy management of a power-split hybrid electric vehicle. *IEEE Transactions on Control Systems Technology*, 20(3).

Camacho, E.F. and Bordons, C. (2007). *Model predictive control*. Springer London.

Clarke, D.W., Mohtadi, C., and Tuffs, P.S. (1987). Generalized predictive control - part 1. the basic algorithm. *Automatica*, 23(2), 137–148.

Fujii, S. and Mizumoto, I. (2017). Adaptive output feedback control with predictive feedforward input based on extended output estimator. *Proceedings of 6th International Symposium on Advanced Control of Industrial Processes (AdCONIP)*, 116–171.

Hara, S., Shen, T., and Zhang, J. (2016). Power demand prediction-based real-time optimal energy management strategy for hevs (in japanese). *Transactions of Society of Automotive Engineers of Japan*, 47(5), 1085–1090.

Huang, Y., Wang, H., Khajepour, A., He, H., and Ji, J. (2017). Model predictive control power management strategies for hevs: A review. *Journal of Power Sources*, 341, 91–106.

Isidori, A. (1995). *Nonlinear Control Systems*. Springer, 3rd edition.

Mizumoto, I., Murakami, S., and Masuda, S. (2018). Aspr based adaptive output feedback control with an output predictive feedforward input for continuous-time systems. *Proc. of the 57th IEEE Conference on Decision and Control*, 613–619.

Nozaki, R., Kawamoto, Y., and Mizumoto, I. (2024). Energy management for a power-split hev based on a robust predictive control (in japanese). *Transactions of the Society of Instrument and Control Engineers (to be published)*, 60(3).

Sciarretta, A. and Guzzella, L. (2007a). Control of hybrid electric vehicle. *IEEE Control Systems Magazine*, 27(2), 60–70.

Sciarretta, A. and Guzzella, L. (2007b). Control of hybrid electric vehicle. *IEEE Control Systems Magazine*, 27(4), 60–67.

Sun, C., Hu, X., Moura, S.J., and Sun, F. (2015). Velocity predictors for predictive energy management in hybrid electric vehicles. *IEEE Transactions on Control Systems Technology*, 23(3), 1197–1207.

Tran, D.D., M.Vafaeipour, Baghdadi, M.E., Barrero, R., Mierlo, J.V., and Hegazy, O. (2020). Thorough state-of-the-art analysis of electric and hybrid vehicle powertrains: Topologies and integrated energy management strategies. *Renewable and Sustainable Energy Reviews*, 119.

Xiang, C., Ding, F., Wang, W., and He, W. (2017). Energy management of a dual-mode power-split hybrid electric vehicle based on velocity prediction and nonlinear model predictive control. *Applied Energy*, 189, 640–653.